Indian Journal of Pure & Applied Physics
Vol. 61, February 2023, pp. 108-114
DOI: 10.56042/ijpap.v61i2.67985

First Principle Study of Electronic, Optical and Thermoelectric Properties of $CuInS_2$ and $CuInSe_2$

Laihnuna* & Z Pachuau

Department of Physics, Mizoram University, Aizawl, Mizoram, 796 004 India

Received 28 October 2022; accepted 18 January 2023

We report the bandgap, thermoelectric and optical properties of $CuInS_2$ and $CuInSe_2$ ternary chalcopyrite compounds based on DFT calculations. Our calculations shows that both $CuInS_2$ and $CuInse_2$ have a direct bandgap which were at the Γ-points. The computed bandgap were 1.35 and 0.85 eV for $CuInS_2$ and $CuInSe_2$. The optical properties analysis shows that the fundamental edge of absorption arise at 0.82 eV and 0.35 eV along the perpendicular and parallel polarization for $CuIns_2$, while it arise at 0.13 eV and 0.16 eV along the perpendicular and parallel polarization for $CuInSe_2$. The static dielectric constant, static refractive index and birefringence were then calculated. The calculated birefringence was negative, which meets the non-critical phase matching (NCPM) requirement, which is beneficial for high-performing laser systems. The optical absorption threshold lies at 1.4 and 0.83 eV for $CuInS_2$ and $CuInSe_2$. These compounds show low reflectivity and high absorption in the visible region. Both compounds have high electrical conductivity and Seebeck coefficient, making them promising candidates for thermoelectric devices.

Keywords: Seebeck coefficient; DFT; Absorption coefficient

1 Introduction

Ternary I-III-VI_2compounds are semiconducting compounds that crystallize into chalcopyrite structures. They have attracted considerable attention because of their excellent absorption coefficients and desirable direct bandgaps for applications in photovoltaics. I-III-VI_2 compounds are promising candidates for applications in solar cells[1-3], light-emitting diodes[4,5] and nonlinear optics[6,7]. Cu-based I-III-VI_2 compounds are especially attractive because of their nontoxicity and high conversion efficiency in solar cells in contrast to lead-based solar cells, which are toxic and not environment friendly. For the purpose of this study, we consider $CuInS_2$ and $CuInSe_2$ because of their technological applications. The direct bandgap and non-cubic structure of $CuInS_2$ lead to interesting electrical and optical properties, including third-order nonlinear optical properties[8-10]. Experimental synthesis of $CuInS_2$ was performed using different methods, and its properties were studied[11,12]. Theoretical studies on the band structure and lattice dynamics of $CuInS_2$ were performed using pseudo potential DFT[13]. The influence of P and In doping on the band structure and stability of $CuInS_2$ has been studied[14]. The structural, dynamical, and dielectric properties of CuInS2 were studied using local density approximation[15]. Theoretical studies of the thermodynamic and elastic properties of CuInS2 have been performed using DFT[16]. $CuInSe_2$ is extensively used in photovoltaic materials because of its large absorption coefficient[17], high conversion efficiency[18], and low production cost[19]. Various experimental studies have been performed to synthesize $CuInSe_2$and better understand its electrical and optical properties at ambient pressure[20-27]. The structure of $CuInSe_2$ changes upon application of pressure, which increases its absorption coefficient[28]. The transport properties of $CuInSe_2$ and $CuInS_2$ are also important parameters that significantly influence its practical applications[29].

2 Computational Details

Calculations were performed within the DFT framework using FP-LAPW as implemented in WIEN 2k[30]. The MBJ[31] potential was used as the exchange-correlation potential to compute the band structure and optical properties. The structures of $CuInS_2$ and $CuInSe_2$ were optimized to obtain stable structures using GGA[32]. For good energy convergence, the cut-off energy was set at -6.0 Ry, 3000 k-points were used, and the cut off plane wave vector in the interstitial region was $R_{MT} \times K_{max} = 8$. A maximum angular momentum quantum value of 10, and Fourier

*Corresponding author: (E-mail: laihnuna20@gmail.com)

charge density of 12Ry were used. The energy and charge convergences were set as0.0001Ry and 0.001e, respectively. The thermoelectric properties were calculated using semi-classical Boltzmann transport theory with a constant τ approximation as implemented in Boltz TraP2[33].

3 Results and Discussion

3.1 Electronic properties

The computed band structures of $CuInS_2$ and $CuInSe_2$ are shown in Fig. 1 (a) and (b). They were computed across the sharp symmetry points of the BZ from Γ to H, N, Γ, and P. The top VB and CB minima were located at the Γ-points of the BZ for $CuInS_2$ and $CuInSe_2$, indicating that both have a direct bandgaps. Fig. 2 shows the computed TDOS and PDOS for better insight into the energy bands. Three sub-bands emerged from the valence bands for both compounds. The upper sub-bands for $CuInS_2$ lies between the fermi energy and -1.7 eV and the lower two sub-bands lies between -3.4 to -5.1 eV and -5.7 to -6.1 eV respectively. The upper sub-band of $CuInSe_2$ lies between the fermi energy and -1.4 eV and the lower two sub-bands lies between -3 to -4.8 eV and -5.4 to -6.3 eV respectively. The highest orbital occupied in the VB was characterized by Cu 3d, S 3p, and Se 4p

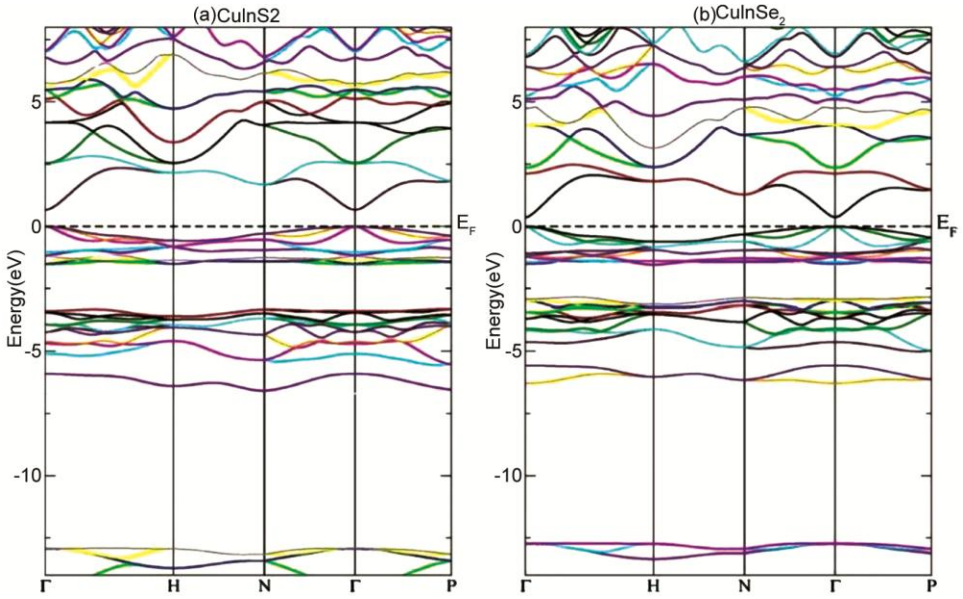

Fig. 1 — Calculated Electronic Band Structure of (a) $CuInS_2$ and (b) $CuInSe_2$.

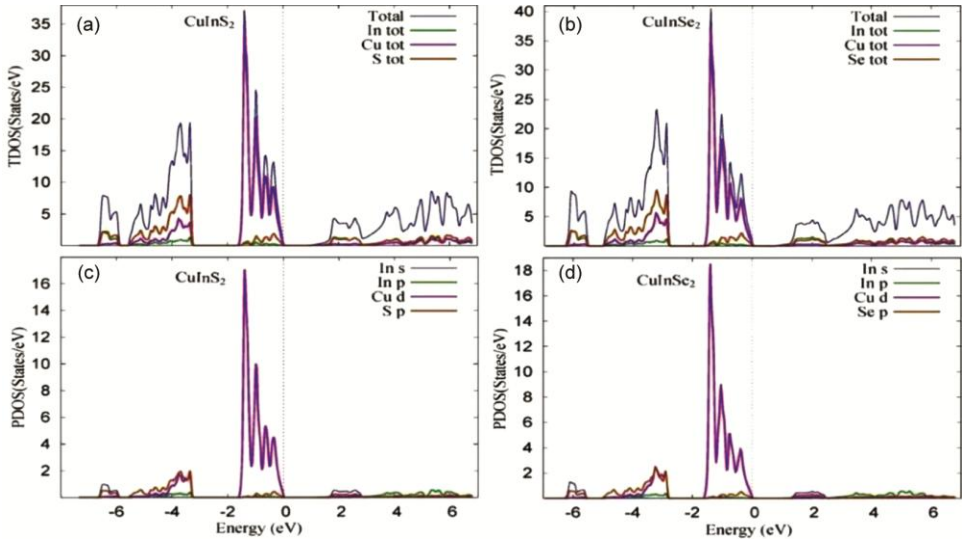

Fig. 2 — Calculated Total and Partial Density of States for $CuInS_2$ and $CuInSe_2$.

states whereas the lower CB was mostly attributed to the In 5s states for $CuInS_2$ and $CuInSe_2$. The upper VB signifies an anti bonding of Se 4p and S 3p states with Cu 3d states, while the CB minima is mostly attributed to the anti bonding of In 5s, Se 4p with S 3p states. The calculated bandgaps is shown in Table 1. The computed bandgap is less than the experimental result indicating the inadequacy of DFT approach for calculating the band structure.

3.2. Optical properties

The linear response of a macroscopic optical properties of a solids are usually described by means of complex dielectric function[34,35] given by

$$\varepsilon(\omega) = \varepsilon_1(\omega) + i\varepsilon_2(\omega) \quad \ldots (1)$$

$\varepsilon_1(\omega)$ and $\varepsilon_2(\omega)$are dispersive and absorptive parts of the complex dielectric function. The imaginary part $\varepsilon_2(\omega)$of dielectric function with appropriate momentum matrix is given by[36]

$$\varepsilon_2(\omega) = \frac{e\hbar}{\pi m^2 \omega^2} \sum_{v,c} \int |M_{cv}(k)|^2 \, \delta\,[\omega_{cv}(k) - \omega] d^3k \quad \ldots (2)$$

$\varepsilon_1(\omega)$ can be obtained from $\varepsilon_2(\omega)$using the Kramer-Kronig transformation[37] as,

$$\varepsilon_1(\omega) = 1 + \frac{2}{\pi} P \int_0^\infty \frac{\omega' \varepsilon_2(\omega')}{\omega'^2 - \omega^2} d\omega' \quad \ldots (3)$$

The other optical parameters such as, reflectivity[38], absorption coefficient (α)[38], refractive index[39] and extinction coefficient[39] can be calculated as follows,

$$R(\omega) = \left| \frac{\varepsilon^{\frac{1}{2}}(\omega) - 1}{\varepsilon^{\frac{1}{2}}(\omega) + 1} \right| \quad \ldots (4)$$

$$\alpha(\omega) = \sqrt{2\omega} \left[\left(\sqrt{\varepsilon_1^2(\omega) + \varepsilon_2^2(\omega)} \right) - \varepsilon_1(\omega) \right]^{\frac{1}{2}} \quad \ldots (5)$$

$$n(\omega) = \left[\frac{\varepsilon_1}{2} + \frac{\sqrt{\varepsilon_1^2(\omega) + \varepsilon_2^2(\omega)}}{2} \right]^{\frac{1}{2}} \quad \ldots (6)$$

$$k(\omega) = \left[\frac{\sqrt{\varepsilon_1^2(\omega) + \varepsilon_2^2(\omega)}}{2} - \frac{\varepsilon_1}{2} \right]^{\frac{1}{2}} \quad \ldots (7)$$

Figure 3 (a) shows the calculated real part of the dielectric function for $CuInS_2$ and $CuInSe_2$. The overall structure of $\varepsilon_1(\omega)$ is similar for both $CuInS_2$ and $CuInSe_2$. There are four main peak located at 0.8, 2, 4.1, and 5.2 eV for $CuInS_2$and four main peaks located at 0.5 eV, 1.6 eV, 4.23 eV and 6.3 eVfor

Table 1 — Calculated Bandgap

Compounds	E_g (eV) Our work	Other Theoretical work	Experimental work
$CuInS_2$	1.35	0.26[a], 0.873[b], 1.37[b]	1.55[c], 1.53[d]
$CuInSe_2$	0.85	0.26[a], 0.748[b], 1.23[b]	1.04[d]

[a]Ref. [44], [b]Ref. [45], [c]Ref [46], [d]Ref [47]

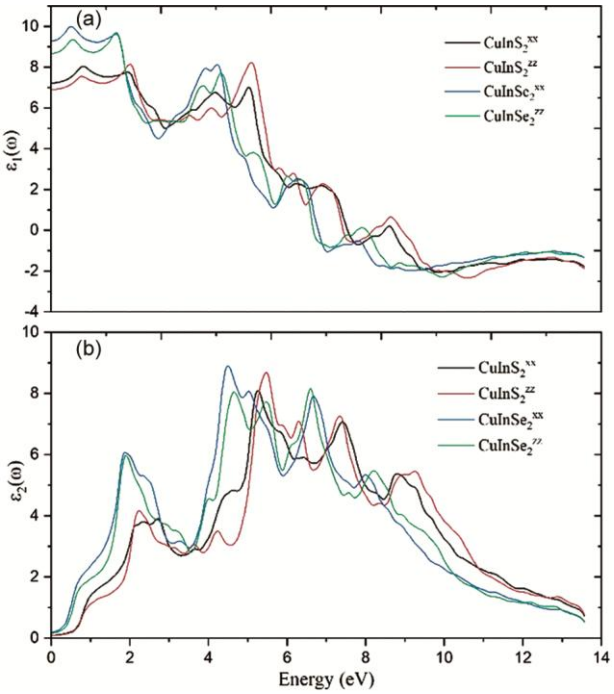

Fig. 3 — Calculated (a) Real and (b) Imaginary parts of Dielectric Function for $CuInS_2$ and $CuInSe_2$.

$CuInSe_2$. These peaks originate from the electronic transitions between the upper VB and the lower CB, andthe peak intensity decreases with increasing energy. The energy at which of $\varepsilon_1(\omega)$is zero in the ultraviolet region indicates the disappearance of the dispersionthat causes absorption. The negative value of $\varepsilon_1(\omega)$indicates the non-propagation of electromagnetic waves in this region and can be used as a shield against electromagnetic waves in this region. The static dielectric constant has an inverse relationshipwith the bandgap, which can be explained using the Penn model[40]. The calculated static dielectric constants are listed in Table 2. The calculated spectra of $\varepsilon_2(\omega)$ for $CuInS_2$ and $CuInSe_2$ are presented in Fig. 3 (b). The fundamental edge of absorption arise at 0.82 eV and 0.35 eV along the perpendicular and parallel polarization for $CuIns_2$, while it arise at 0.13 eV and 0.16 eV along the perpendicular and parallel polarization for $CuInSe_2$. The fundamental edge corresponds to a transition

Table 2 — Calculated static dielectric constant

	Our Work		Other Work	
Compounds	$\varepsilon^{xx}(0)$	$\varepsilon^{zz}(0)$	$\varepsilon^{xx}(0)$	$\varepsilon^{zz}(0)$
$CuInS_2$	7.23	6.91	7.51[a], 8.6[b], 9.71[c]	6.97a, 8.4[b], 9.68[c]
$CuInSe_2$	9.29	8.67	9.86[a], 11[b]	8.95[a], 10.8[b]

[a]Ref [48], [b]Ref [49], [c]Ref [15]

Table 3 — Calculated static refractive index with birefringence

	Our Work			Other Work		
Compounds	$n^{xx}(0)$	$n^{zz}(0)$	$\Delta n(0)$	$n^{xx}(0)$	$n^{zz}(0)$	$\Delta n(0)$
$CuInS_2$	2.69	2.62	-0.07	2.76[a],	2.6[a],	-0.16[a],
$CuInSe_2$	3.04	2.94	-0.1	3.17[a],	3.01[a],	-0.16[a],

[a]Ref [48]

between the lowest CB and highest VB. Beyond the threshold energy, three main peaks are located at 2.74, 5.26, and 7.41 eV for $CuInS_2$. These peaks originate from the transitions of the hybridized bonding of S 3p and Cu 3d states.Beyond the threshold energy three main peaks are located at 1.86, 4.5 and 6.6 eV for $CuInSe_2$. These peaks are mainly attributed to the transitions of hybridized bonding ofSe 4pandCu 3d states. These peaks correspond to region of strongest absorption of, and the first peak liesin the visible region and extends all the way to the ultraviolet region. Peaks with lower amplitude arise owing to the nature of hybridization of π and σ bonding and the anti-bonding of Cu 3d states ans the S 3p and Se 4p states.

Figure 4 (a) shows the calculated refractive index for $CuInS_2$ and $CuInSe_2$. The refractive index describe the macroscopic polarization of a material due to an incident electromagnetic waves. Two main peaks were observed in the refractive index spectra. The first peak lies in the infrared region, whereas the second peak lies in the ultraviolet region.$n(\omega)$ exhibits anisotropy that results in birefringence, which accounts for the prominent nonlinear optical properties of these compounds. The extent of birefringence, which is given by $\Delta n = n^{\parallel} - n^{\perp}$, along with the static refractive index, is listed in Table 3. $\Delta n(0)$ is negative for both compounds, which meets the non-critical phase matching (NCPM) requirement, which is beneficial for high-performing laser systems. Figure 4 (b) shows the calculated extinction coefficient for $CuInS_2$ and $CuInSe_2$. The extinction coefficient spectra of $CuInS_2$ and $CuInSe_2$ are almost identical because of the similarity in their band structures. Both compounds has intense peak between 4.8 eV to 8.5 eV. The intensity of the peak exhibits a red shift and it decrease with increase in energy. This indicates that the electric field vanished

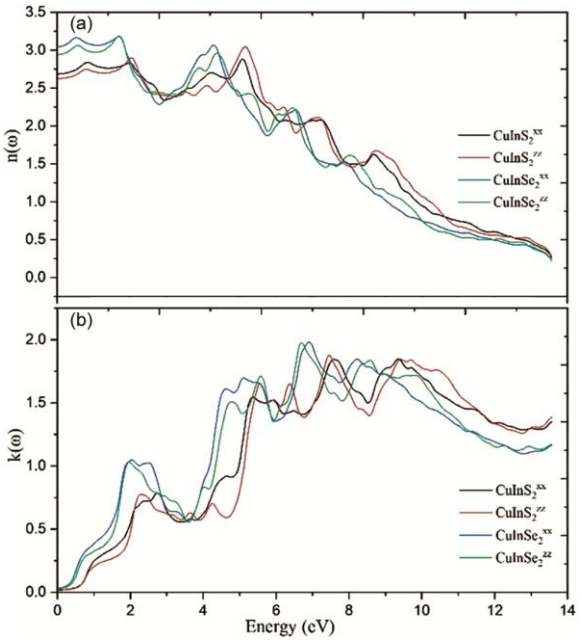

Fig. 4 — Calculated (a) Refractive index and (b) Extinction coefficient for $CuInS_2$ and $CuInSe_2$.

with respect to the incident energy. k(ω) represents damping of the oscillating electric field amplitude. Three sharp peaks appears around 5.34 eV, 7.5 eV and 9.34 eV for $CuInS_2$ and at 5.1 eV, 6.8 eV and 8.2 eV for $CuInSe_2$, indicating region of strongest absorption. The extinction coefficient decreased after reaching a peak owing tolow absorption. The correlation between the absorption and extinction coefficients can be explained using Beer-Lambert law[41].

Figure 5 (a) shows the calculated absorption coefficients of $CuInS_2$ and $CuInSe_2$.Optical absorption is an important optical parameter that displays the luminosity arising from electronic transitions. The absorption coefficient provides information on the number of electromagnetic waves with distinct

energies that enter a material prior to absorption. The incident photons may be absorbed through direct or indirect transitions, depending on whether the energy gap is lower than the incident radiation energy. The absorption threshold lies at 1.4 eV and 0.83 eV for $CuInS_2$ and $CuInSe_2$ which are in good agreement with other calculation at 1.5eV[42] for $CuInS_2$ and 0.83 eV[43] for $CuInSe_2$. The absorption has maxima of 175.7 x 10^4 and 186.6 x 10^4 cm^{-1} located at 9.4 eV and 10.4 eV along the perpendicular and parallel directions for $CuInS_2$ while the absorption has maxima of 157.8 x 10^4 and 171.8 x 10^4 cm^{-1} located at 9.1 and 9.8 eV along the perpendicular and parallel directions for $CuInSe_2$. The absorption coefficient strongly increases with increasing energy, indicating the beginning of a direct transition. The reflectivity spectra of $CuInS_2$ and $CuInSe_2$ are shown in Fig. 5 (b). The reflectivity intensify along the infrared region and then decrease as it approach the visible region. The static reflectivity was 20% and 21 % along the perpendicular and parallel polarizations for $CuInS_2$while the static reflectivity for $CuInSe_2$ was 26 % and 24% along the perpendicular and parallel polarizations. The reflectivity exhibited the highest intensity in the ultraviolet region for both compounds, which can be utilized to create Bragg's reflectors.

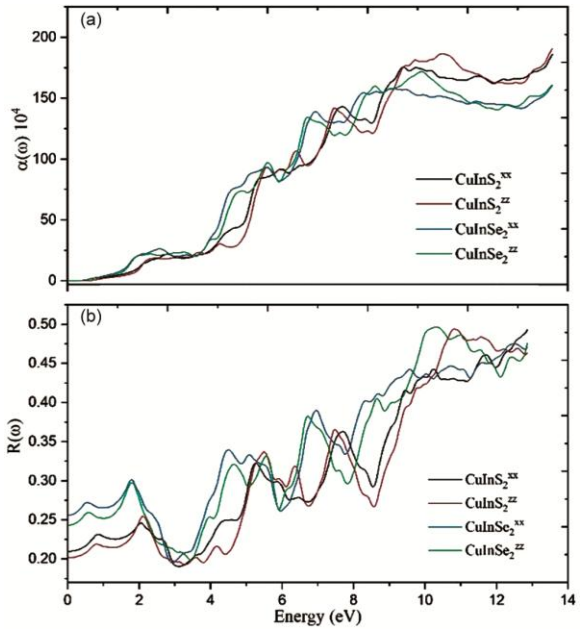

Fig. 5 — Calculated (a) Adsorption coefficient and (b) Reflectivity for $CuInS_2$ and $CuInSe_2$.

3.3. Thermoelectric properties

The thermoelectric properties of $CuInS_2$ and $CuInSe_2$ were calculated using semi-classical Boltzmann transport theory, as implemented in BoltzTraP2[33]. τ (relaxation time) was assumed to be constant. The thermal conductivity due to lattice vibrations was not considered when calculating ZT. The calculated electrical conductivity is shown in Fig. 6 (b). The increase in temperature causes easier movement of the carriers from the VB to the CB, resulting in an increase in σ/τ with temperature. The calculated $(\sigma/\tau)^{xx}$ and $(\sigma/\tau)^{zz}$ for $CuInS_2$ at room temperature were 8.55 x 10^{19} $(\Omega ms)^{-1}$ and 6.84 x 10^{19} $(\Omega ms)^{-1}$. For $CuInSe_2$, the calculated $(\sigma/\tau)^{xx}$ and $(\sigma/\tau)^{zz}$ values at room temperature were 7.76 x 10^{19} $(\Omega ms)^{-1}$ and 5.74 x 10^{19} $(\Omega ms)^{-1}$. The Seebeck coefficient is a measure of the magnitude of change in induced

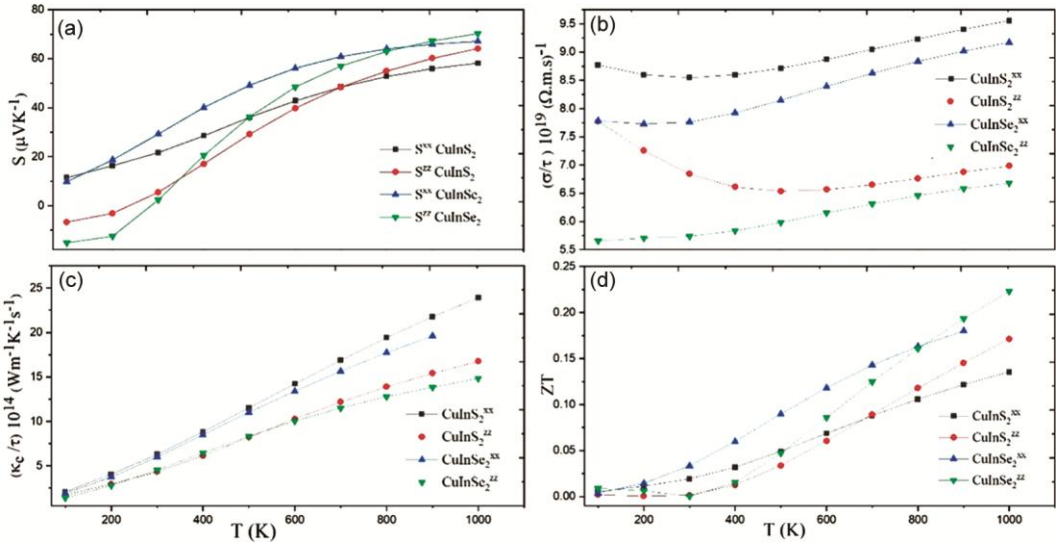

Fig. 6 — Calculated (a) Seebeck coefficient (b) Electrical conductivity (c) Thermal conductivity and (d) Figure of merit for $CuInS_2$ and $CuInSe_2$.

voltage with respect to the change in temperature, given by $S = \Delta V/\Delta T$[50]. Fig. 6 (a) shows the variations of S (Seebeck coefficient) with temperature. The Seebeck coefficient increased linearly as the temperature increase 100 K to 1000 K for both compounds. The calculated S^{xx} and S^{zz} for $CuInS_2$ at room temperature were 21.7 $\mu VK^{-1}$and 5.43 μVK^{-1} respectively. For $CuInSe_2$ the calculated S^{xx} and S^{zz} at room temperature were 29.32 μVK^{-1} and 2.32 μVK^{-1}. A positive Seebeck coefficient indicated the presence of p-type carriers. Both compounds have high electrical conductivity with a high Seebeck coefficient at room temperature, which is characteristic of good thermoelectric materials.

Thermal conductivity is attributed to electronic and lattice vibrations, which constitute the total thermal current. The contribution of the lattice vibrations was ignored in the calculations. The calculated thermal conductivities are shown in Fig. 6 (c). The calculated $(\kappa_e/\tau)^{xx}$ and $(\kappa_e/\tau)^{zz}$ values for $CuInS_2$ at room temperature were 6.29 x $10^{14}$and 4.32 x $10^{14}Wm^{-1}K^{-1}s^{-1}$, respectively. For $CuInSe_2$ the calculated $(\kappa_e/\tau)^{xx}$ and $(\kappa_e/\tau)^{zz}$ at room temperature were 5.9 x $10^{14}$and 4.5 x $10^{14}Wm^{-1}K^{-1}s^{-1}$. The relationship between electrical conductivity and thermal conductivity is given by the Wiedemann-Franz law $LT= \kappa/\sigma$[51]. To obtain good thermoelectric materials, this ratio must be small. The κ/σ ratios for $CuInS_2$ and $CuInSe_2$ were quite small, of the order 10^{-5}, making them good candidates for thermoelectric devices. The efficiency of the thermoelectric material was assessed using the dimensionless figure of merit $ZT= S^2\sigma T/\kappa$[52]. Ideally thermoelectric materials should exhibits ZT values near or greater than unity. The variation of ZT with temperature is shown in Fig. 6 (d). It increased linearly with temperature. The value of ZT at room temperature were 0.019 and 0.034 for $CuInS_2$ and $CuInSe_2$ respectively. The calculated ZT at room temperature is quite low, although the Seebeck coefficient and σ/τ are high. This was owing to the exclusion of lattice thermal conductivity for calculating the figure of merit.

4 Conclusions

We investigate bandgap, optical parameters, and thermoelectric properties of $CuInS_2$ and $CuInSe_2$ ternary chalcopyrite compounds based on DFT calculations. Three sub-bands emerged from the valence bands for both compounds. The upper sub-bands for $CuInS_2$and$CuInSe_2$lie between the fermi energy and -1.7 eV and -1.4 eV respectively. Our calculations shows that both $CuInS_2$ and $CuInse_2$ have a direct bandgap which were at the Γ-points. The computed bandgaps were of 1.35 eV and 0.85 eV for $CuInS_2$ and $CuInSe_2$.The calculated bandgap is less than the experimental result indicating the inadequacy of DFT approach for calculating the energy bands. The real part of the dielectric function of $CuInS_2$ and $CuInSe_2$ has four main peak located at 0.8 , 2 , 4.1, and 5.2 eV for $CuInS_2$ and the main peak for $CuInSe_2$ are located at 0.5, 1.6, 4.23, and 6.3 eV. The calculated $\varepsilon(0)$ and $n(0)$ were compared with available experimental and theoreticaldataand are in reasonable agreement. The fundamental edge of absorption arise at 0.82 eV and 0.35 eV along the perpendicular and parallel polarization for $CuIns_2$, while it arise at 0.13 eV and 0.16 eV along the perpendicular and parallel polarization for $CuInSe_2$.$\Delta n(0)$ was negative for both compounds, which meets the non-critical phase matching (NCPM) requirement, which is beneficial for high-performing laser systems. The extinction coefficient exhibits three sharp peaks appears around 5.34 eV, 7.5 eV and 9.34 eV for $CuInS_2$and at 5.1 eV, 6.8 eV and 8.2 eV for $CuInSe_2$, indicating region of strongest absorption. The absorption threshold lies at 1.4 and 0.83 eV for $CuInS_2$ and $CuInSe_2$. Both compounds exhibit high Seebeck coefficient and electrical conductivity, making them promising candidates for thermoelectric devices.

References

1 Chirila A, Reinhard P, Pianezzi F, Bloesch P, Uhl A R, Fella C, Kranz L, Keller D, Gretener C & Hagendorfer H, *Nature Mater*, 12 (2013) 1107.

2 Rau U & Schock H W, *Appl Phys A*, 69 (1999) 131.

3 Contreras M A, Egaas B, Ramanathan K, Hiltner J, Swartzlander A, Hasoon F, Noufi R, *Prog Photovolt*, 7 (1999) 311.

4 Wagner S, Shay J L, Tell B & Kasper H M, *Appl Phys Lett*, 22 (1973) 351.

5 Shay J L, Schiavone L M, Wernick J H & Buehler E, *J Appl Phys*, 43 (1972) 2805.

6 Levine B F, *Phys Rev B*, 7 (1973) 2600.

7 Ohmer M C, Goldstein J T, Zelmon D E, Saxler A W, Hegde S M, Wolf J D, Schunemann P G & Pollak T M, *J Appl Phys*, 86 (1999) 94.

8 Du J J, *Mater Rev*, 21 (2007) 9.

9 LI J, Mo X L, Sun D L & Chen G R, *Acta Physico-Chimica Sinica*, 25 (2009) 2445.

10 Sun Q, *J Artif Cryst*, 42 (2013) 65.

11 Wang Z D, *Vacuum*, 48 (2011) 29.

12 Feng L, *J Chem*, 69 (2011) 2870.

13 Łażewski J, Jochym P T & Parlinski K, *The J Chem Phys*, 117 (2002) 2726.

14 Yamamoto T & Katayama-Yoshida H, *J Ternary Multinary Compounds*, (2020) 37.
15 Eryiğit R & Parlak C, *Eur Phys J B-Condens Matter Comp Syst*, 33 (2003) 251.
16 Fan S & Lu Z, *Thermal Science*, 00 (2021) 302.
17 Diao C C, Kuo H H, Tzou W C, Chen Y L & Yang C F, *Materials*, 7 (2014) 206.
18 Schmid D, Ruckh M, Grunwald F & Schock H W, *J Appl Phys*, 73 (1993) 2902.
19 Kapur V K, Basol B M & Tseng E S, *Solar cells*, 21 (1987) 65.
20 Panthani M G, Akhavan V, Goodfellow B, Schmidtke J P, Dunn L, Dodabalapur A & Korgel B A, *J Am Chem Soc*, 130 (2008) 16770.
21 Abou-Ras D, Schäfer N, Rissom T, Kelly M N, Haarstrich J, Ronning C & Rollett A D, *Acta Materialia*, 118 (2016) 244.
22 Maeda T, Gong W & Wada T, *Jpn J Appl Phys*, 55 (2016) 04ES15.
23 Maeda T & Wada T, *Jpn J Appl Phys*, 49 (2010) 04DP07.
24 Belhadj M, Tadjer A, Abbar B, Bousahla Z, Bouhafs B & Aourag H, *Physica Status Solidi (b)*, 241 (2004) 2516.
25 Houck D W, Assaf E I, Shin H, Greene R M, Pernik D R & Korgel B A, *The J Phys Chem C*, 123 (2019) 9544.
26 Chugh M , Kühne T D & Mirhosseini H, *ACS Appl Mater Interfaces*, 11 (2019) 14821.
27 Persson C & Zunger A, *Phys Rev Lett*, 91 (2003) 266401.
28 Gonzalez J & Rincon C, *J Appl Phys*, 65 (1989)2031.
29 Errandonea D, Segura A, Martínez-García D & Muñoz-San Jose V, *Phys Rev B*, 79 (2009) 125203.
30 Blaha P, Schwarz K, Madsen G H, Kvasnicka D & Luitz J, FP-L/APW+lo Program for Calculating Crystal Properties, Techn WIEN2K, Austria, 2001.
31 Tran F, Tran F & Blaha P, *Phys Rev Lett*, 102 (2009) 226401.
32 Perdew J, Burke K P & Ernzerhoff M, *Phys Rev Lett*, 77 (1996) 3865.
33 Madsen G K, Carrete J & Verstraete M J, *Comput Phys Commun*, 231 (2018) 140.
34 Kramers H A, (Transactions of Volta Centenary Congress), *Atti Cong Intern Fisica* 2 (1927) 545.
35 Kronig R D L, *J Opt Soc Am A*, 12 (1926) 547.
36 Ambrosch-Draxl C & Sofo J O, *Comput Phys Commun*, 175 (2006) 1.
37 Reshak A H, Fedorchuk A O, Lakshminarayana G, Alahmed Z A, Kamarudin H & Auluck S, *Comput Mater Sci*, 78 (2013) 134.
38 Ziane M I, Bensaad Z, Labdelli B & Bennacer H, *Sensors Transduc*, 27 (2014) 374.
39 Cheddadi S, Boubendira K, Meradji H, Ghemid S, Hassan F, Lakel S & Khenata R, *Pramana*, 89 (2017) 89.
40 Penn D R, *Phys Rev*, 128 (1962) 2093.
41 Swinehart D F, *J Chem Edu*, 39 (1962) 333.
42 Soni A, Gupta V, Arora C M, Dashora A & Ahuja B L, *Sol Energy*, 84 (2010) 1481.
43 Nayebi P, Mirabbaszadeh K & Shamshirsaz M, *Phys B: Condens Matter*, 416 (2013) 55.
44 Belhadj M, Tadjer A, Abbar B, Bousahla Z, Bouhafs B & Aourag H, *Phys Status Solidi (b)*, 241 (2004) 2516.
45 Ghosh A, Thangavel R & Rajagopalan M, *J Mater Sci*, 50 (2015) 1710.
46 Tell B, Shay J L & Kasper H M, *Phys Rev B*, 4 (1971) 2463.
47 Jaffe J E & Zunger A, *Phys Rev B*, 27 (1983) 5176.
48 Amudhavalli A, Rajeswarapalanichamy R, Padmavathy R, Manikandan M, Santhosh M, & Iyakutti K, *Mater Today Commun*, 26 (2021) 101790.
49 Marquez R & Rincon C, *Physica Status Solidi (b)*, 191 (1995) 115.
50 Noor N A, Saddique M B, Haq B U, Laref A & Rashid M, *Phys Lett A*, 382 (2018) 3095.
51 Takeuchi T, *Mater Trans*, 50 (2009) 0908170873.
52 Tritt T M & Rowe D, *Thermoelectrics Handbook: Macro to Nano*, (2005).